Supporting Online Material for

DNA Binding Site Sequence Directs Glucocorticoid Receptor Structure and Activity

Sebastiaan H. Meijsing, Miles A. Pufall, Alex Y. So, Darren L. Bates, Lin Chen, Keith R. Yamamoto*

*To whom correspondence should be addressed. E-mail: yamamoto@cmp.ucsf.edu

Published 17 April 2009, *Science* **324**, 407 (2009)
DOI: 10.1126/science.1164265

This PDF file includes:

Materials and methods

Plasmids.

Glucocorticoid receptor (GR) binding site (GBS) reporters were constructed using oligonucleotides encoding the GBS sequences as indicated in Fig. 1, with overhangs to facilitate direct cloning into the *Kpn*I and *Xho*I sites of pGL3-Promoter (Promega). Vectors for GR expression, osteocalcin and composite GilZ GRE reporters have been described previously *(S1-3).* The three GBSs of the composite GilZ GRE reporter were changed to a different GBS sequence by site directed mutagenesis (see Fig. S3). The GRγ expression construct was made by PCR-mediated insertion of 3 base pairs using pcDNA3-ratGR *(S1)* as a template. Site directed mutagenesis was used to construct other receptor mutants with primer sequences available upon request. The pET28a vector (Novagen) was used to express the GR DNA binding domain (GR-DBD, amino acids 440-525 and human GR-DBD, amino acids 380-540).

Transient transfections.

For reporter activity assays, U2OS cells were seeded into 24-well plates in DMEM/5% FBS at approximately 20,000 cells per well and transfected the following day in FBS-free DMEM using 0.8 μl of Lipofectamine and 1.6 μl of PLUS reagent (Invitrogen) per well according to manufacturer instructions. Cells were transfected with 20 ng of receptor and reporter, 100 ng empty plasmid p6R, and 20 ng of lacZ or pCMV-Renilla. After transfection (3 h), cells were re-fed with DMEM/5% FBS, allowed to recover for 3 h, and re-fed with DMEM/5% FBS containing 100 nM dex or ethanol. Approximately twelve hours later cells were lysed in 100 μl per well of 1x lysis buffer (PharMingen) and assayed for luciferase and β-galactosidase activity as described (*S4*). For Renilla normalized assays, the Dual-Luciferase Reporter kit was used (Promega) and activities were read in a 96-well format using a plate reader (Tecan). A549 cells were transfected as described for U2OS cells with the following exceptions: 4 times the amount of DNA was used, and cell were transfected using Lipofectamine 2000 (Invitrogen) according to the technical manual.

Cell lines.

A549 and U2OS cells were grown in 5% FBS. To generate stable GRγ cell lines, parental U2OS cells (ATCC no. HTB-96), which do not express endogenous GR, were transfected with the pcDNA3-GRγ expression vector. The next day, cells were trypsinized and transferred to 15-cm dishes and resistant clones were selected at 750 μg/ml G418 (Invitrogen). Isolated colonies were expanded and tested for GR expression by indirect immunofluorescence and immunoblotting with the GR-specific polyclonal antibody N499. Clones homogeneously expressing GR mutants at levels similar to those of WT GR in a U2OS-rGR line (*S5*) were further analyzed. Cells expressing either GRα or GRγ

were treated with 0.01% ethanol vehicle or 100 nM dexamethasone for 4 h and total RNA was isolated as described previously (*S1*). Reported expression data for differentially expressed GRα and GRγ target genes was confirmed in independent clonal cell lines.

Immunoblotting.
Total proteins from equal amounts of cells were separated with SDS page gels, transferred to polyvinylidene difluoride (PVDF) membranes (Millipore) and incubated with anti-GR (N499), anti-Brm (BD transduction), anti-CARM1 (AB-228, Imgenex), anti-actin (SC-1616R, Santa Cruz Biotechnology) or anti-Hsp90 (SC-13119, Santa Cruz Biotechnology) antibodies, followed by an incubation with the appropriate secondary antibody conjugated with horseradish peroxidase. An ECL detection system (Amersham Biosciences) was used to visualize the proteins.

Lentiviral shRNA.
Lentiviruses (*S6*) were used to knockdown expression Brm or Carm1. The lentiviruses were produced with PCR products containing the U6 promoter and the shRNA of interest (*S7*). Target sequence for Carm1: AAGGGTTCACCTCACACTTGAA; for Brm: AAGGAGGTGCTAAGACACTTATG; Scrambled sequence: AAGGGTAGGTTCGACTAGCAGGACTCT. The PCR products were subcloned into the pHRCMVPUROWSin18 vector and subsequently transfected into HEK293 T cells along with pMD.G1 and pCMVDR8.91 (generously provided by Dr. Didier Trono, University of Geneva). After 48 hr and 72 hr, the culture medium containing the shRNAs expressing lentivirus was harvested. After infection, A549 cells were selected with 4μg/ml puromycin. Approximately one week after infection, knockdown was confirmed at mRNA and protein level and reporter constructs of interest were transfected and analyzed as described above.

Quantitative Real Time PCR (qPCR).
RNA isolation, reverse transcription and qPCR were performed as previously described (*S1*). Briefly, total RNA was isolated from cells by using RNeasy Mini kits (Qiagen). Random-primed cDNA was prepared from 1 μg of total RNA by using the ProtoScript first-strand cDNA synthesis kit (New England Biolabs). Approximately one fiftieth of the resultant cDNA was used per reaction using primer pairs as described (*S1, S8*) or as listed in Table 1. Data were analyzed by using the Ct method (Applied Biosystems Prism 7700 Users Bulletin No. 2) using Rpl19 as an internal control for data normalization.

Chromatin Immunoprecipitation (ChIP).
ChIP assays using the N499 GR-antibody, were performed as described (*S8, S9*). Cells were treated for 2 h with 100 nM dexamethasone and precipitated

DNA fragments were analyzed by qPCR using primers as described (*S8*), and data were normalized to hsp70.

Electrophoretic Mobility Shift Assays (EMSA).

EMSAs were performed to determine the DNA binding-affinity of the GR-DBD. Briefly, the binding sites (see Fig. 1) were embedded in complementary cy-5 end-labeled oligonucleotides (for example GilZ GBS: GTACAGAACATTGGGTTCCCTGA). A series of protein dilutions were mixed with 2 x 10^{-10} M DNA in 20 mM Tris pH 7.5, 2 mM MgCl2, 1 mM EDTA, 10% glycerol, 0.3 mg/ml BSA, 4 mM DTT, 0.1 μg/μl dIdC. Reaction mixes were incubated for 30 minutes to reach equilibrium, loaded onto running 8% native gels and scanned using a Typhoon (Amersham) to quantify free [D] versus total $[D]_t$ DNA. Equilibrium binding constants (K_D) were measured by non-linear least squares fitting of the free protein concentration [P] versus fraction of DNA bound ($[PD]/[D]_t$) to the equation $[PD]/[D]_t = 1/(1+(K_D/[P]))$ using Kaleidagraph (v 3.51, Synergy Software).

Protein expression and purification.

The DNA binding domain of rat GRα and GRγ (GR-DBD and GRγ-DBD 440-525) and human GRα (380-540) embedded in a pET28a vectors (Novagen) were expressed in BL21 Gold cells (Stratagene). Protein expression was induced for 4 hrs (optical density ~0.7) with 0.5 mM IPTG at 30°C. Cells were spun down and resuspended in 20ml/L of cells of lysis buffer: 50mM Tris (pH 8.0), 500mM NaCl, 15 mM Imidazole, 1 mM PMSF. Lysate was centrifuged for 1 hr at 40,000 rpm, 4°C and loaded onto a Ni Sepharose (GE Healthcare) column equilibrated with lysis buffer and eluted with a linear gradient to 350mM Imidazole. Protein containing fractions were pooled, and the his_6 tag removed by adding $CaCl_2$ to 2.5 mM and 1unit/mg Thrombin while dialyzing into: 20mM Tris (pH 7.5), 40mM NaCl, 2.5 mM CaCl2, 1mM DTT at 4°C. Precipitate was removed after dialysis by centrifugation, 40 minutes, 40,000 rpm at 4°C. Further separation was achieved by running the supernatant over a SourseS column and eluting with a shallow gradient from 50 to 300mM NaCl in 20mM Tris (pH 7.5) with 1 mM DTT. As a final purification step, the GR-DBD containing fractions were pooled and concentrated then run over 16/60 Superdex75 gel filtration column equilibrated in 20mM Hepes (pH 7.7), 100mM NaCl and 1 mM DTT.

Crystallization.

GR-DBD:DNA and GRγ-DBD:DNA complexes were made by mixing protein and DNA at a 2:1 molar ratio, with DNA starting at approximately 1mM. Single strands of DNA were ordered (IDT), then purified over a 10/10 MonoQ column using a 0.5M to 0.85M NaCl gradient in 10mM NaOH, dialyzed extensively against water, lyophilized, then resuspended in water to a concentration of 2mM. Strands were then mixed with their complement in 20mM HEPES (pH 7.7) 100mM NaCl, boiled for 5 minutes and annealed overnight to

room temperature. GR-DBD was concentrated to between 0.6 and 1.5mM using 5,000 MWC Amicon Ultra concentrators, spun down at maximum speed for 15 minutes at 4°C in a microfuge, then mixed with DNA. Particularly at higher concentrations, the complexes would begin to precipitate upon mixing. Addition of 5M ammonium acetate to a final concentration of 0.4M often alleviated this problem and aided in crystallization. Complexes were then crystallized using the Natrix (Hampton Research) or Nucleix (Qiagen) screens by hanging drop. Crystals were typically transferred to solutions containing 30% ethylene glycol, looped, and frozen in liquid nitrogen.

Structure determination.

Data sets for the crystals were collected at the Advanced Light Source, Lawrence Berkeley National Labs (ALS). Native data sets were collected at 1.11 Å (beam line 8.3.1), or 1 Å (beam lines 5.0.2, 8.2.1, 8.2.2), whereas anomalous data sets were collected at the Zn^{2+} edge, 1.283 Å, at all beamlines. In order to determine the orientation of DNA in the crystals, we ordered HPLC purified version of the top strand of Pal, FKBP, GilZ and Sgk with a BrdU substituted for T at the 6 position. Anomalous data sets taken at the Br edge (0.92 Å, ALS beamlines 8.3.1 and 5.0.2), then used to generate anomalous difference Fourier maps using the CCP4 suite of programs (*S10*).

Images were processed and scaled using HKL2000. The Phenix suite of programs were then used to generate phased maps (AutoSol), molecular replacement solutions (AutoMR), simulated annealing and composite-omit maps (AutoBuild), positioning of riding hydrogens (phenix.reduce), and for model refinement (phenix.refine) (*S11*). Rfree was generated by setting aside either 10% or 2000 reflections (for data sets less than or greater than 20,000 unique reflections, respectively). The program Coot was used for electron density map examination, model building, positional refinement, and validation (*S12*). Models were further validated using the Molprobity server (*S13*). Data collection and refinement statistics are listed in Table S2. Three dimensional models and figures were generated using either Chimera or PyMol (*S14, S15*).

A phased map of the complex was derived from single anomalous diffraction (SAD) data sets taken at the Zn^{2+} fluorescence absorption edge of the highest resolution GBS16 data set (GR-DBD:Sgk) and GBS18 (GR-DBD:FKBP5) using AutoSol in Phenix (*S11*). Once refined, this model was used to solve the remaining structures by molecular replacement. Accuracy of the models was then verified by examination against composite omit maps.

The complexes align in the crystal using an extensive protein:protein interface as well as non-Watson-Crick base pairing. The DNA forms a pseudocontinuous helix through the crystal. The complexes containing 16bp complexes crystallized in space group C_12_1, and rather than aligning head to tail taking advantage of the engineered A:T overhangs for stability, it is modeled to align head-to-head and tail-to-tail, with an intrusion of an additional A into the duplex to make dual AA:AA pairs at the 5' end, flipping out the most 3' T of the

complimentary strand (Fig. S4). The complexes containing 18bp DNA duplexes crystallized in space group $P2_12_12_1$ and also formed pseudocontinuous helices in the crystal. However, similar to PR-DBD:DNA complexes solved using the same length DNA, the ends again do not take advantage of the complimentary overhangs, but instead form a triple base pair from an intra-duplex Watson-Crick G:C base pair and a Hoogsteen inter-duplex C:G (*S16*).

The BrdU substitution for T6 generated anomalous difference Fourier maps, which revealed that the DNA duplex is not fixed in the 16bp crystals, but distributed equally between forward and reverse orientations. Despite this, even in the case of the palindromic sites (Pal and FKBP5), the protein monomers do not adopt identical conformations – perhaps accentuated by the protein:protein interfaces in the crystal.

Fluorescence anisotropy.

The affinity of GR-DBD wild-type, R510A, and K514A were measured using fluorescence anisotropy. 40μM stock Pal, GilZ, or scrambled GBSs were generated mixing complimentary 23bp duplexes labeled at one end with fluorescein. The
duplexes were then boiled for 5 minutes and slow annealed overnight in a buffer containing 20mM HEPES (pH 7.7) and 500mM NaCl. Duplexes were then diluted to 2nM in binding buffer: 20mM HEPES (pH 7.7), 100mM NaCl, 5mM $MgCl_2$, 200μg/ml BSA, 100μg/ml poly dIdC, 5% glycerol, and 1mM DTT. Protein stocks were prepared in the same buffer to an initial concentration of 20μM, then stepwise diluted 1.5 fold to cover a range from 20μM to 2nM. 20μl of protein and DNA were then mixed in a 96-well plate and incubated for 1 hour at 20°C. The parallel and perpendicular fluorescence was then measured using a TECAN plate reader, and the anisotropy calculated using the following formula:

$$A = (I_{parallel} - I_{perpendicular})/(2I_{perpendicular} + I_{parallel})$$

The resulting signmoidal curves were then fit to an exponential using the statistical program R to determine the K_D.

Supplemental text

Sequence directs differential employment of activation domains in complex context of GRE.

To test if the GBS sequences contribute to defining the regulatory programs within the more complex context of a composite Glucocorticoid response element (GRE), we used a luciferase reporter driven by a 1 kb genomic fragment encompassing the GilZ GRE (*S3*) and tested whether the pattern of GR domain utilization was similar to that of the endogenous GilZ gene (*S1*). The pattern was sufficiently similar (Fig. S3) that we then tested whether mutating the three GBS sequences within the 1 kb GRE would

produce changes in domain utilization. We mutated each of the GBSs to a sequence that evokes a different domain pattern and found that when we mutated all three GBSs, the pattern indeed changes with these modest sequence changes, implying that precise GBS sequences are determinants of GR function even when embedded within complex composite elements. Given that the reporters are identical, except for the sequence of the GBS, our data suggest that the GBS sequence encodes information that influences the function and or composition of the transcriptional complexes formed at GR target genes.

Composite omit maps

Most of the structures were solved by molecular replacement. In order to ensure that we had built these models free from bias, we calculated composite omit maps from the original scaled intensity files using Phenix (specifically, phenix.autobuild: https://www.phenix-online.org/documentation/autobuild.htm). Briefly, composite omit maps are generated by the assembly of a series volumes in the unit cell for which the electron density has been calculated using reflection amplitudes and existing phases (*S17*). In this way, the model does not influence the map. This technique has been used to detect errors in model building, but in this case revealed density that was not apparent in refined maps.

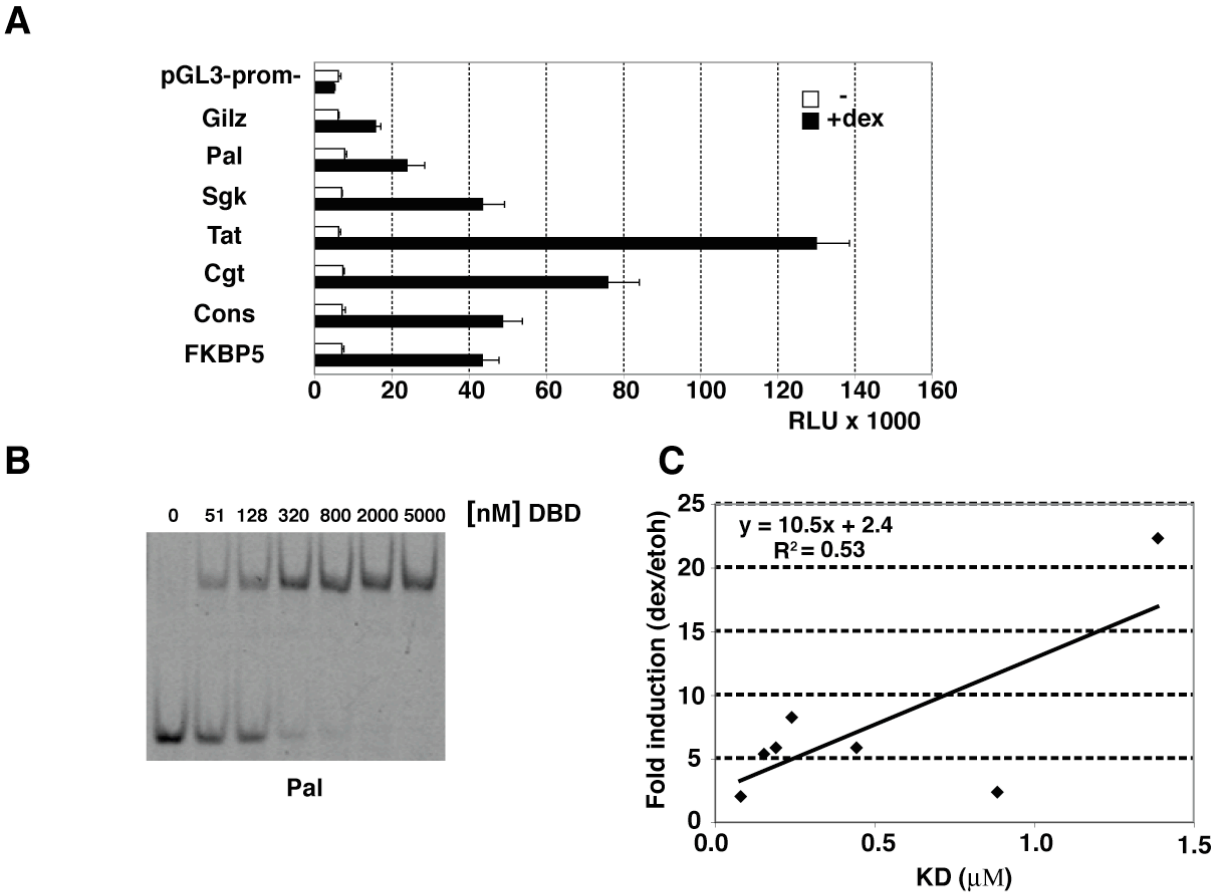

Figure S1. GR binding sites (GBSs) display different regulatory efficacies and binding affinities. (A) The transcriptional activities for GR binding site reporters in the presence or absence of ligand (dexamethasone (dex)). Relative light units ± standard error of the mean (S.E.M.) are shown ($n \geq 3$) (B) Representative gelshift assay showing GR-DBD (human residues 380-540) binding to Pal GBS. (C) Scatter Plot showing the relationship between activity and affinity (hGR DBD 380-540) for the GBSs used in our studies and the coefficient of determination (R^2).

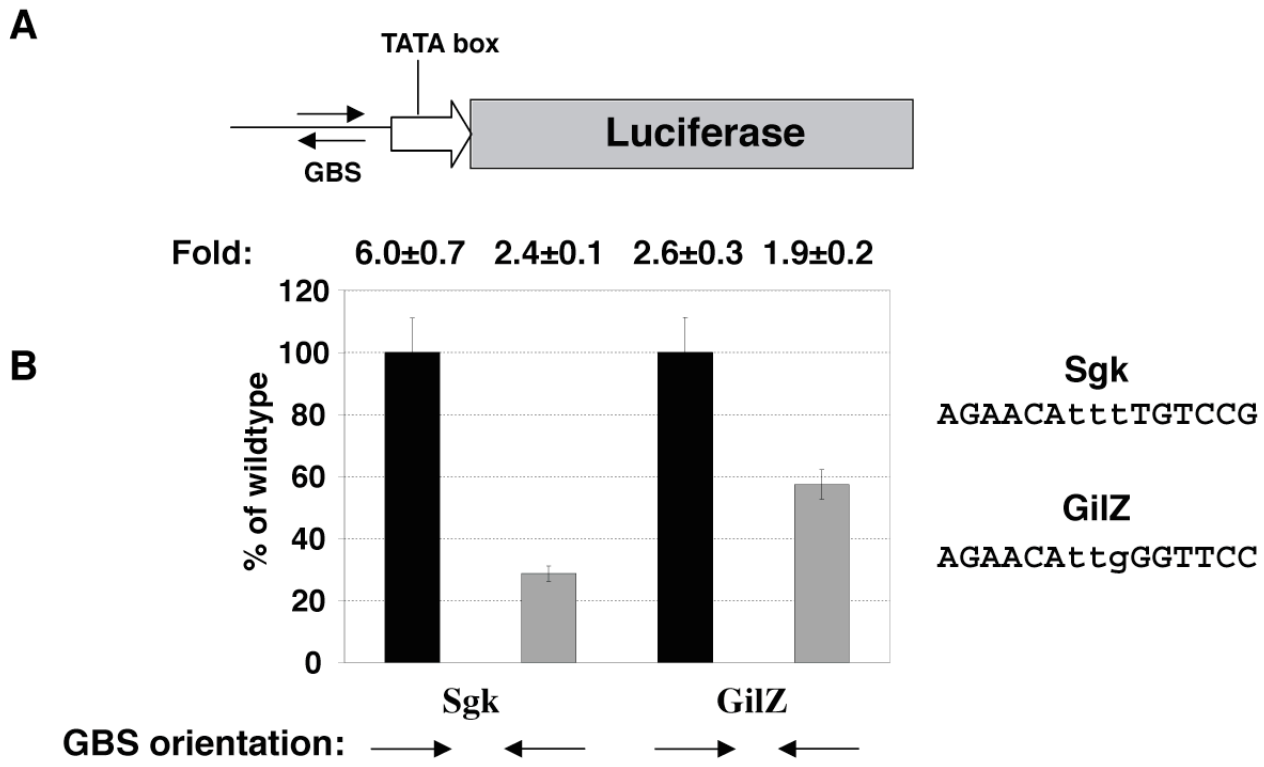

Figure S2. GBS orientation affects transcriptional activity. (A) GBSs were cloned in two orientations upstream of a minimal SV40 promoter driving the expression of a luciferase reporter gene. (B) The transcriptional activities for the orientation with the AGAACA half site distant from the TATA box was set at 100%, and activity of the other orientation displayed as a percentage thereof (fold activation ± S.E.M shown on top of graph (n = 3)).

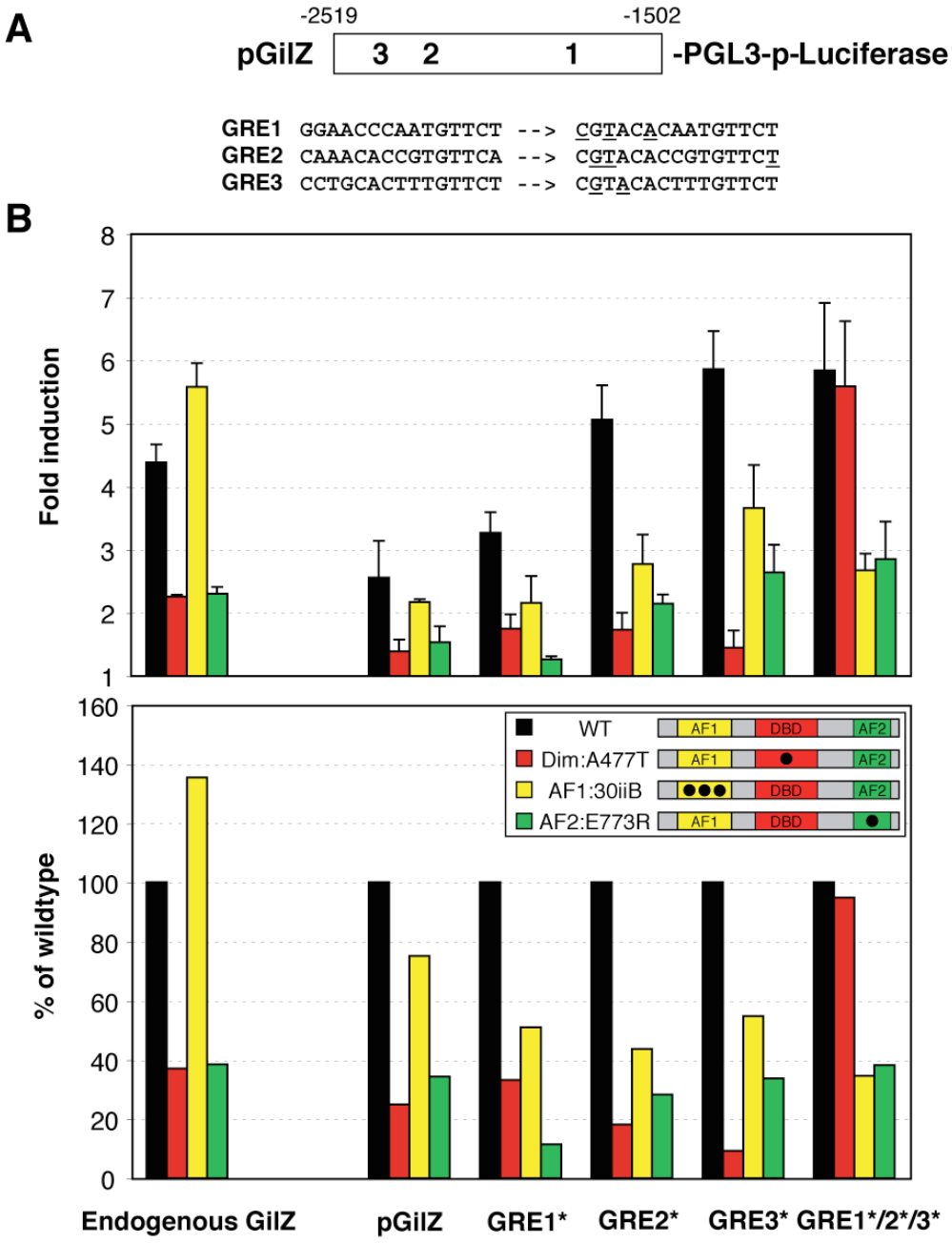

Figure S3. Role of GBSs at a composite GilZ GRE. (A) GilZ reporter with three endogenous GBSs. Shown are the original (left) and mutated (right) sequence with mutated nucleotides underlined. (B) Pattern of domain requirements for the endogenous GilZ gene, the GilZ enhancer reporter construct, and the reporter constructs with GBS sequences altered (GBS*) as indicated in (A). Fold induction upon treatment with hormone (middle) and percentage induction relative to WT (bottom) ± S.E.M. are shown (n ≥ 3).

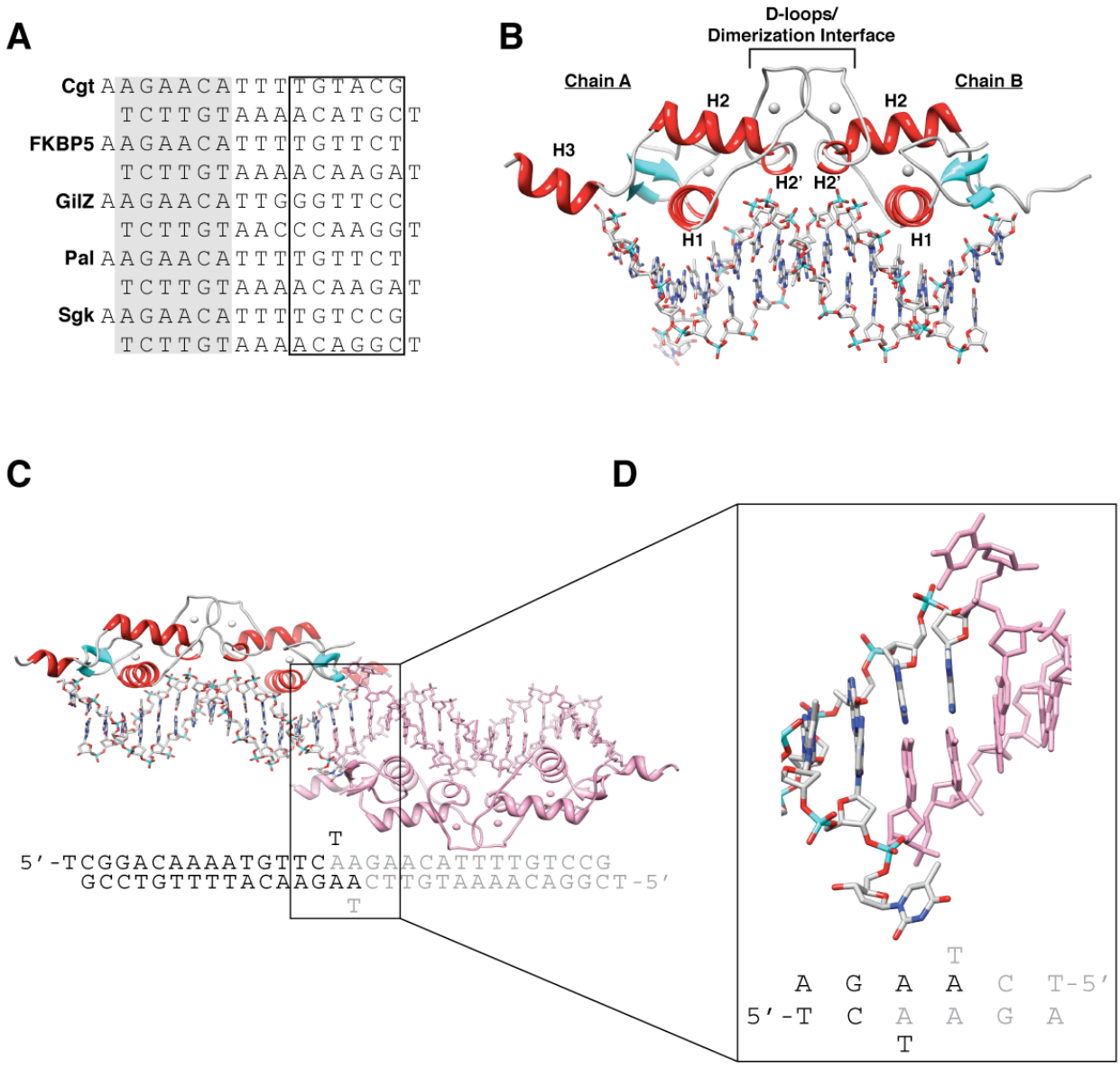

Figure S4. Structure of the glucocorticoid receptor DNA binding domain on a natural GR DNA binding site. (A) Sequence of the GBSs as used for the crystallization studies with A:T overhangs, conserved half site (gray box), and variable half site (boxed). (B) Crystal structure of the DBD bound to Pal sequence with secondary structural elements, as well as chains A and B highlighted. (C) Overview of arrangement of complexes in the crystal highlighting base pairing of neighboring (D) DNAs that form a pseudo-continuous helix.

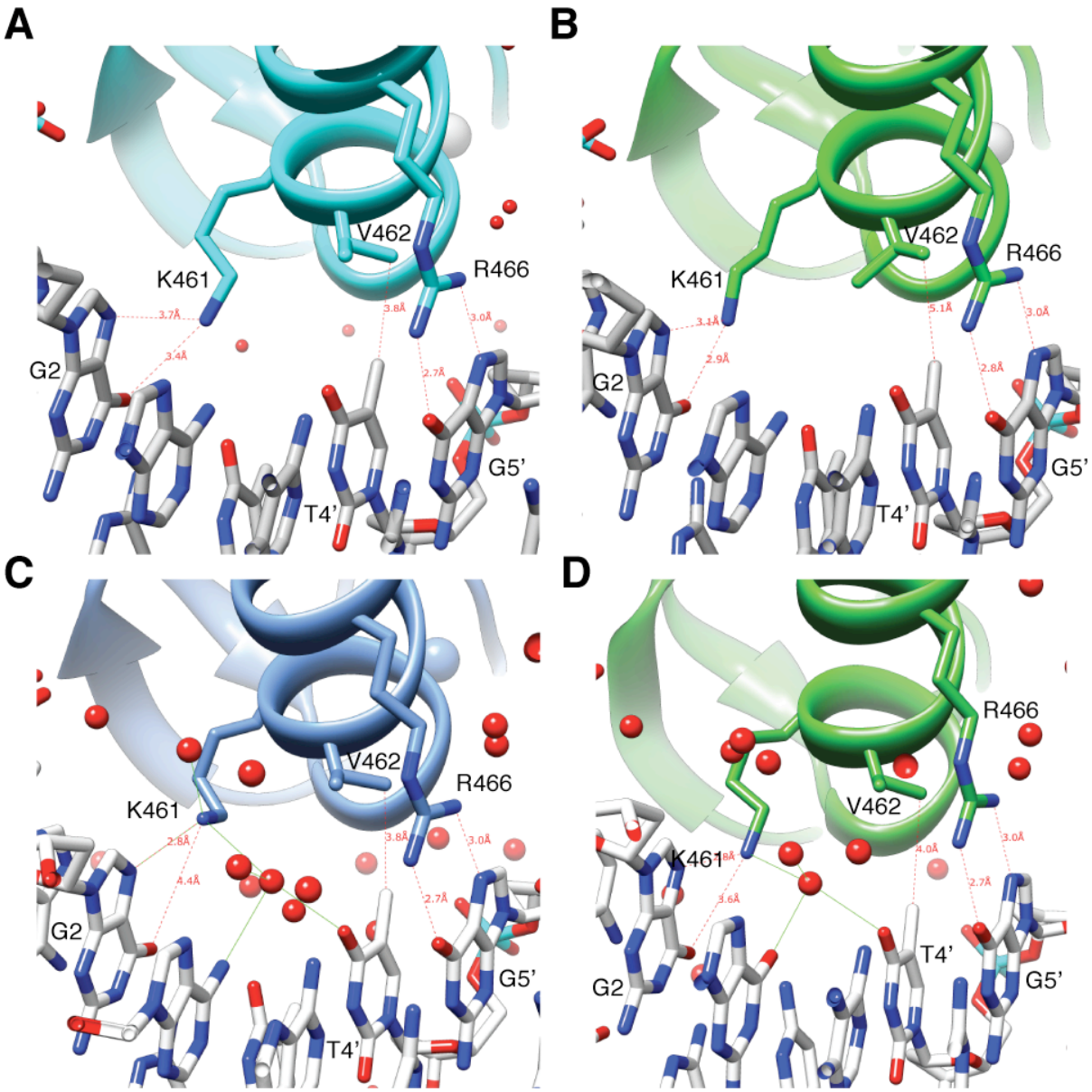

Figure S5. Side chain differences of GR-DBD residues that interact directly with binding site sequences. (A and B) Residues K461, V462, and R466 of the GR-DBD:Pal chain A make specific contacts with base G2, T4' opposite conserved A4, and G5' opposite conserved C5. The contacts made by chain B (B) of GR-DBD:Pal differ from those made by chain A (A). The distance between V462 and the methyl of T4' appears to be too long to make a strong van der Waals contact, and the positioning of K461 indicates a stronger interaction with G2. (C and D) The higher resolution GR-DBD:Sgk structure shows different positioning of specific contacts in the major groove, particularly by K461, for chains A (C) and B (D). The terminal amine of K461 is repositioned and poised to make water mediated contacts, perhaps extending which bases are recognized beyond G2, T4', and G5'.

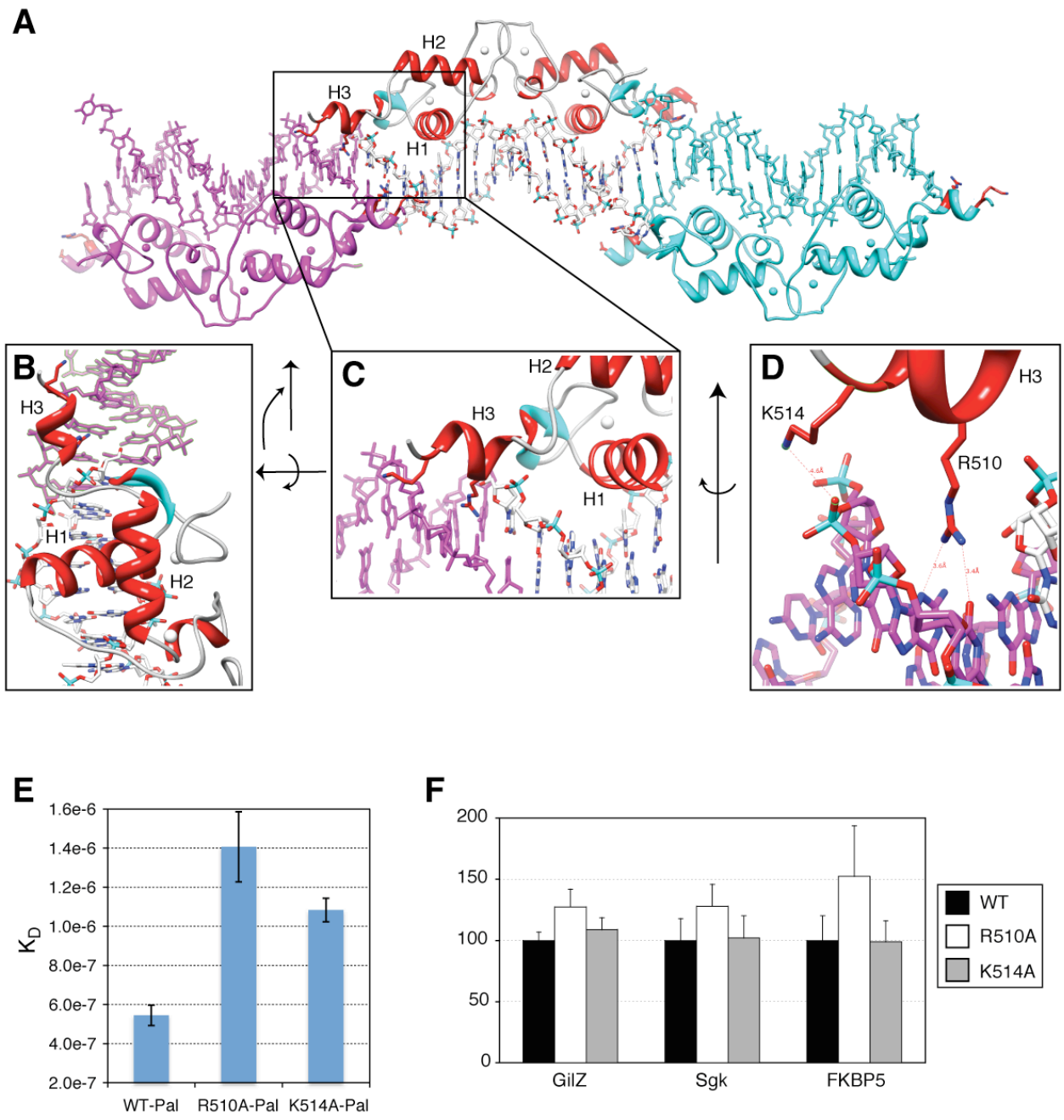

Figure S6. Structure and function of C-terminal extended helix (H3). (A-C) Views of N-terminal H3 helix from different angles. (D) Minor groove contacts by K514 and R510 of helix H3. (E) Affinities (μM) of wild-type, R510A, and K514A mutants for the Pal GBS were determined by fluorescence anisotrophy. Averages ± S.E.M are shown (n = 3). (F) The transcriptional activities for GBS reporters of GR, R510A, and K514A mutants as percentage of wild-type activity ± S.E.M (n ≥ 3).

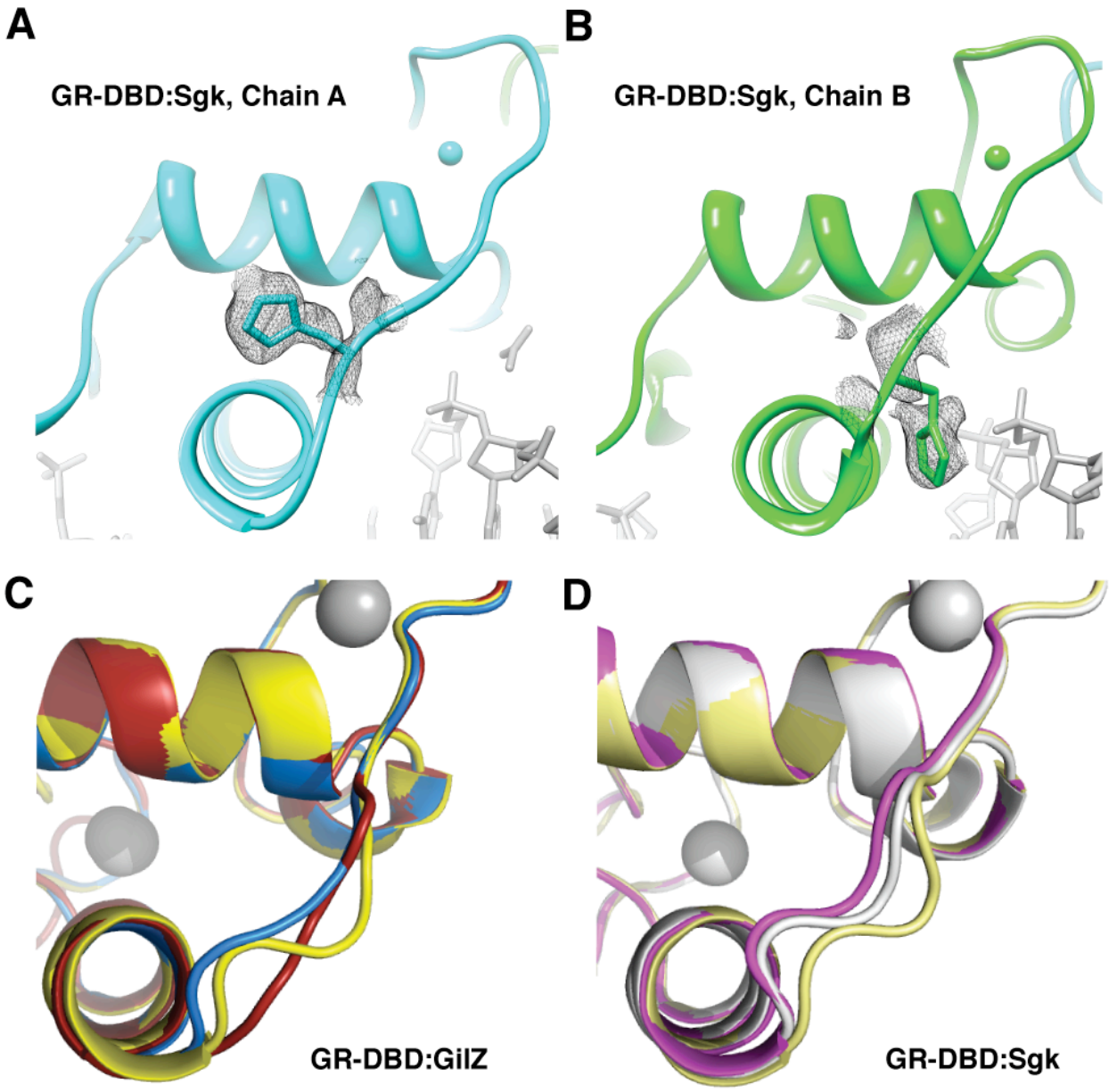

Figure S7. Changes in the lever arm conformation. (A and B) Simulated annealing omit maps superimposed on the lever arm of GR reveal two distinct orientations of H472 in chain A (packed) and chain B (flipped), respectively. (C) Crystallization conditions induce different conformations within the chain B lever arm when bound to the GilZ GBS (See Materials and Methods for crystallization conditions). (D) The GBS Sgk directs a single conformation within the chain B lever arm, as evidenced by comparison of structures solved from crystals from three different crystallization conditions.

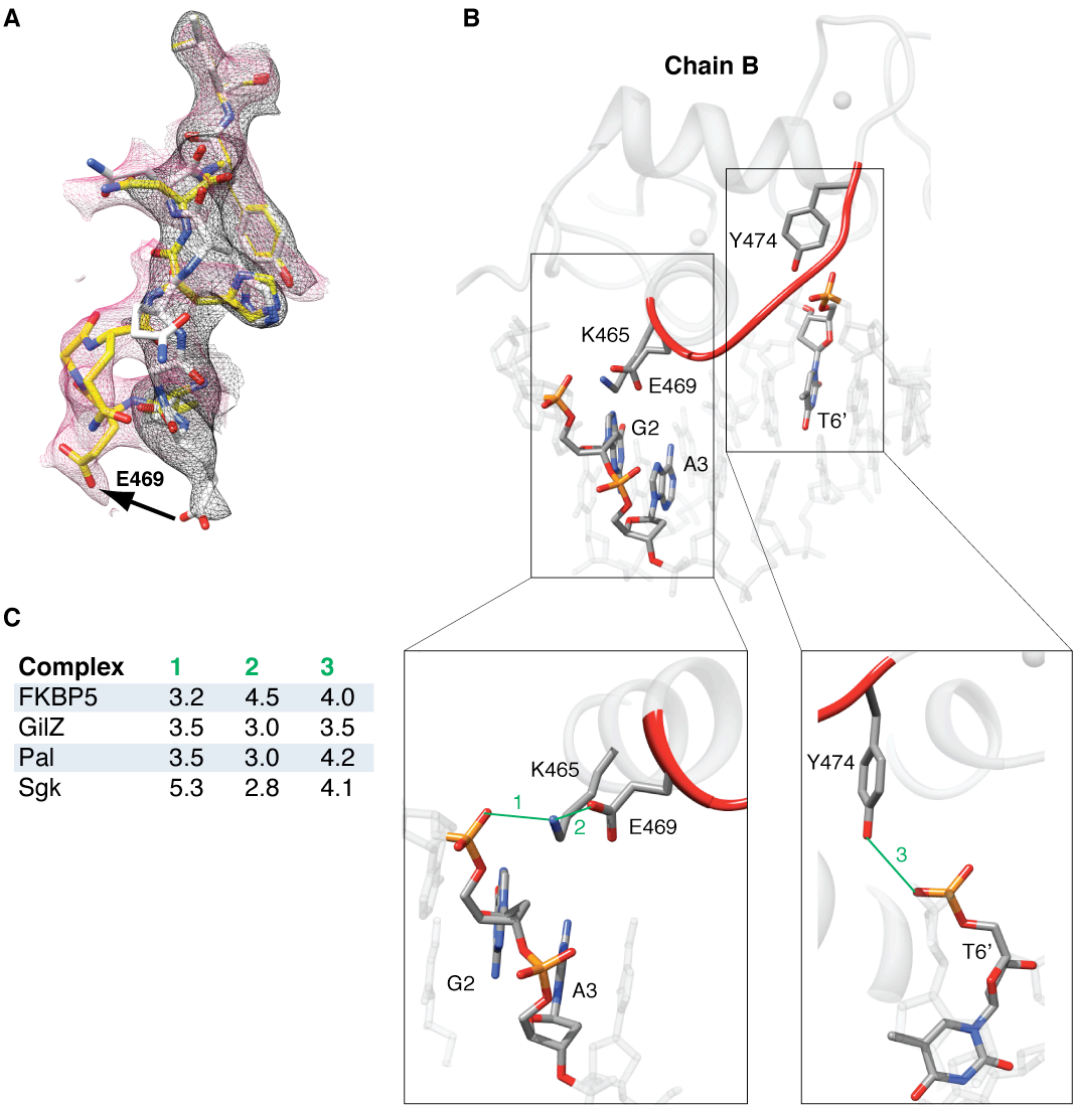

C

Complex	1	2	3
FKBP5	3.2	4.5	4.0
GilZ	3.5	3.0	3.5
Pal	3.5	3.0	4.2
Sgk	5.3	2.8	4.1

Figure S8. DNA backbone contacts restrict the lever arm. (A) In the GR-DBD:FKBP5 complex, E469 is displaced in the alternative conformation (yellow) of the lever arm defined by the composite omit map (red mesh). (B) The lever arm is anchored by DNA backbone contacts. E469 makes an indirect contact with the backbone through K465. (Left inset; Distance 2, shown in green) to form a hydrogen bond with a phosphate oxygen of either G2 (Distance 1) or, in some cases, A3. (Right inset) At the other end of the lever arm, Y474 has the potential to interact with a phosphate oxygen of T6' (Distance 3). (C) Distances measured from crystal structures formed under the same conditions indicate that GilZ is unique among the complexes in forming contacts at both ends of the lever arm. Anchoring both ends to DNA may restrict the lever arm to adopt a unique conformation.

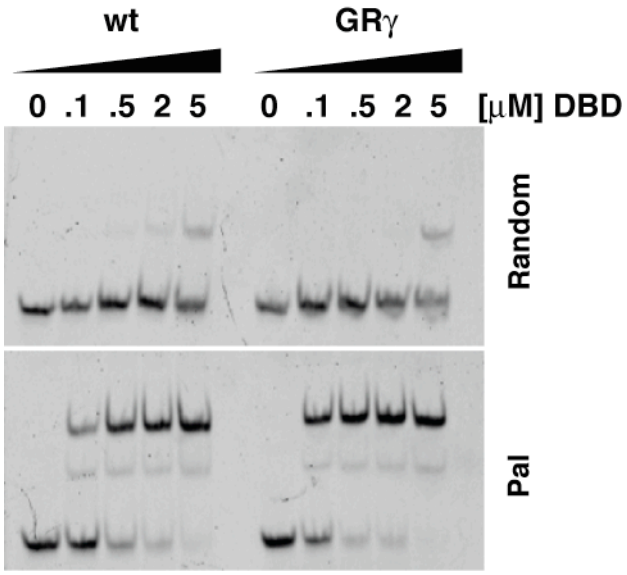

Figure S9. GRα and GRγ bind DNA with comparable affinities. Gel shift assays showing GRα-DBD or GRγ-DBD binding to the Pal GBS or to randomized sequences.

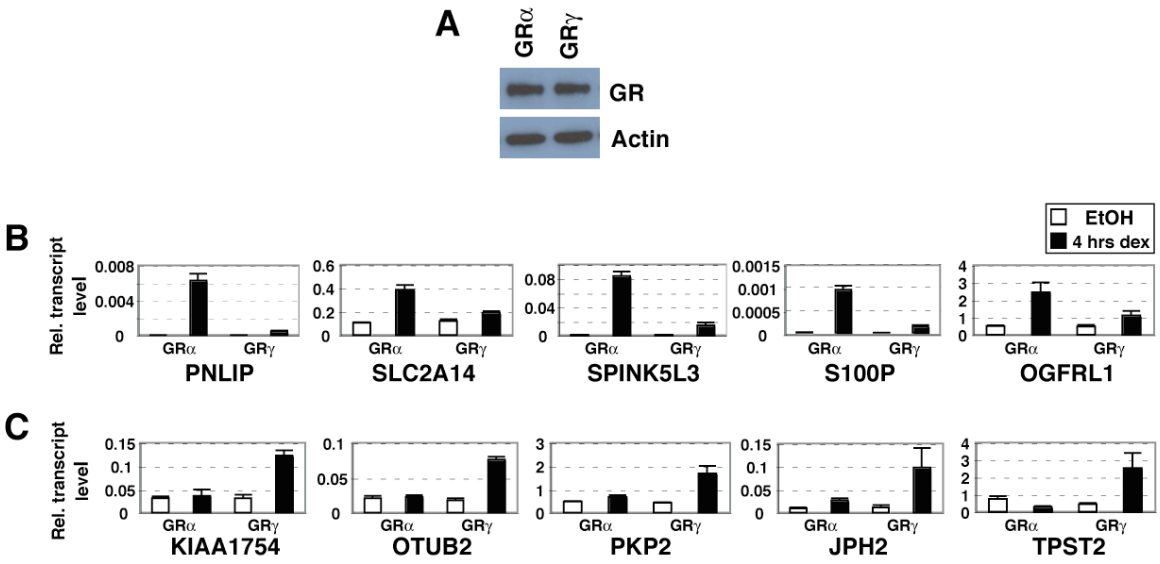

Figure S10. Isoform-specific regulation of endogenous target genes. (A) Expression levels of GR in U2OS cells stably expressing GR isoforms was analyzed by immunoblotting with antibodies against GR and actin as a control for loading. (B) GRα-specific target genes. (C) GRγ-specific target genes. Relative transcript levels of treated (4h, 100nM dex) or untreated cells expressing GRα or GRγ were analyzed by real-time quantitative PCR. Averages ± S.E.M are shown (n = 3).

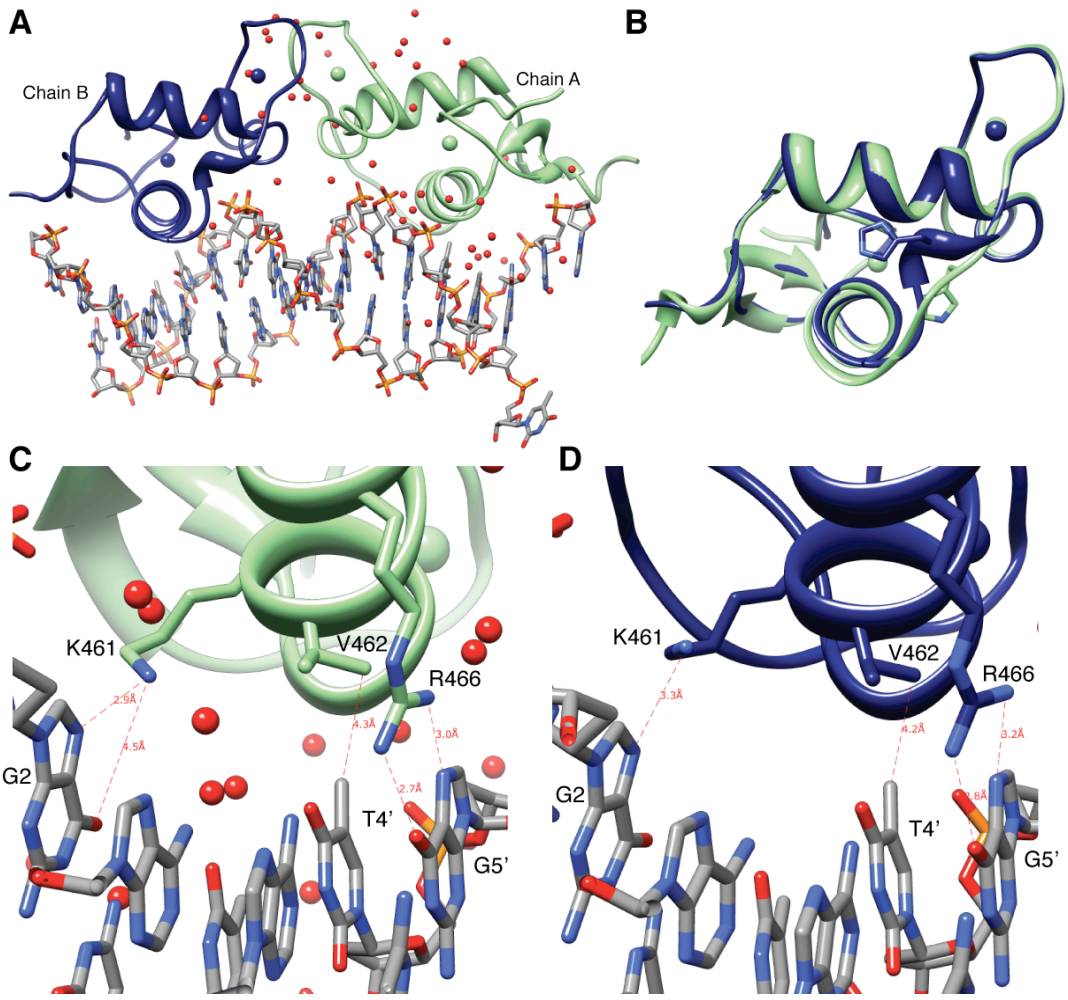

Figure S11. GRγ structure and base contacts. (A) The structure of the GRγ-DBD bound to the FKBP5 16bp sequence is shown. The model has been flipped from convention to show chain B (Navy Blue) on the left and chain A (Light Green) on the right. The lever arm of the free chain B contains an α-helical twist upon insertion of the single Arg residue. (B) An overlay of chains A and B with H472 represented in stick form. Neither lever arm in the GRγ structure adopts the packed conformation. Instead, H472 of chain A resembles the unpacked conformation of the wild type, and H472 of chain B flips out to make contacts with an adjacent complex in the crystal (contacts not shown). (C) Despite insertion of a residue within the lever arm, the specific base contacts made are similar to those observed for wild type: residue K461 forms a hydrogen bond to the N7 of G2; V462 makes a van der Waals contact with the methyl group of T4' (opposite the conserved A4 in the GBS half site); R466 makes bidentate hydrogen bonding contacts with G5' (opposite the conserved C5 in the GBS half site) for both chain A (C) and chain B (D).

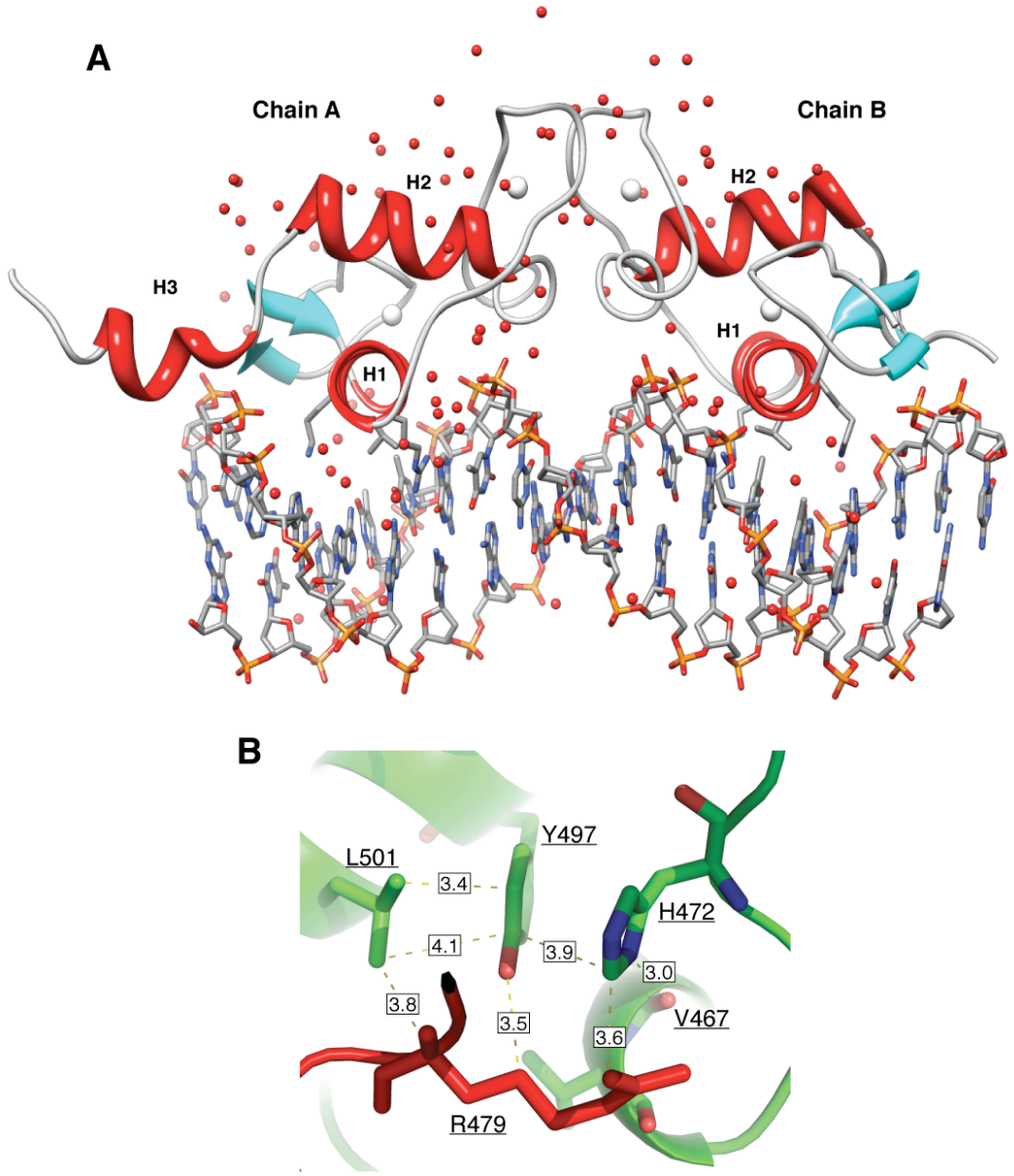

Figure S12. GBS18 structure and H472 packing. The structure of GR-DBD bound to an 18bp version of FKBP5 is shown. The protein conformation is essentially identical to that solved on the 16bp GBS, with all secondary structural elements intact. (A) The DNA forms a continuous pseudo-helix through the crystal without any bases flipping out, but bound to the neighboring complex though Hoogsteen triple base pairing (not shown). (B) H472 of the lever arm once again adopts the packed conformation in chain A, interacting with V467 and Y497, which is in turn aligned by L501. V497 and L501 are unique to GR, as is the residue neighboring V467, L468. These interactions are trapped by R479 from an adjacent complex in the crystal.

Table S1. Primers used for qPCR analysis.

Gene:	Forward primer:	Reverse Primer:
PNLIP	gatgttggggacttgcagat	aacttcctccctgacggttt
SLC2A14	accggcttcctcattacctt	ttggtggtggtctccttagc
SPINK5L3	ctgcctttccccacaagatt	ttgaggcacaaacaggtgct
OGFRL1	ccactgaagcaactgccaaa	caccatctggcttgaatgga
KIAA1754	agtctggcccagttcagaga	cgctggagtgaggaactagg
OTUB2	ctgctgaaggtgttcaacga	gaagtgccggaagaagtctg
PKP2	gcctatgcctccaacaaagc	gtggtaggctttggcagtcc
JPH2	caccaccaccgagacctaca	cttggtgtccttgaccagca
TPST2	gcatggaggtaggcaaggag	ggcttgccaatgaggtcttc

Table S2. Crystallographic Data.

GR-DBD:GBS 16 bp Complexes (Part 1)

Data	**Cgt**	**FKBP5**		**GilZ**		
Crystal Condition[a]	47	9	49	5	9	65
Wavelength (Å)	1.11	1.11	1.11	1.11	1.11	1.11
Space Group	C_12_1	C_12_1	C_12_1	C_12_1	C_12_1	C_12_1
α (°)	90	90	90	90	90	90
β (°)	123.5	122.1	122.7	123.5	122.9	123.2
γ (°)	90	90	90	90	90	90
a (Å)	117.5	116.0	116.2	116.9	116.8	117.2
b (Å)	37.8	38.9	39.1	38.6	38.6	37.9
c (Å)	96.7	95.5	95.6	98.5	97.1	97.0
Resolution (Å)	50-1.9 (1.95-1.85)[b]	50-2.4 (2.43-2.34)	40-1.95(2.03-1.94)	50-2.0 (2.10-2.02)	50-2.25 (2.34-2.24)	50-2.1 (2.15-2.10)
# unique reflections	28,466	14,217	25,139	24,639	17,393	19,599
Completeness (%)	96.7(81)	93.5(68)	92.1(69)	99.3(95.2)	93.7(71)	94.1(75)
I/σ	16.4(2.2)	20.4(4.4)	19.2(2.1)	23.1(4)	16.6(3.3)	16.6(2.1)
R_{merge}	0.103(0.43)	0.075(0.311)	0.052(0.336)	0.064(0.45)	0.063(0.321)	0.063(0.364)
Refinement						
R_{work}/R_{free}	17.9/21.9	17.2/21.4	18.9/22.0	21.5/24.5	20.6/24.9	20.9/25.7
B factor	57.7	68.76	81.4	83.0	85.2	84.4
RMS bond length	0.010	0.010	0.013	0.011	0.011	0.010
RMS bond angle	1.32	1.482	1.507	1.416	1.436	1.323

[a] Crystal condition corresponds to corresponding number in the Nucleix Suite (Qiagen).
[b] Numbers in parentheses are for highest resolution shell.

GR-DBD:GBS 16 bp Complexes (Part 2)

Data	**Pal**		**Sgk**			
Crystal Condition	9	35	7	9	44 (Native)	44 (SAD)
Wavelength (nm)	1.00	1.11	1.00	1.00	1.00	1.283
	$C_1 2_1$	$C_1 2_1$	$C_1 2_1$	$C_1 2_1$	$C_1 2_1$	$C_1 2_1$
α (°)	90	90	90	90	90	90
β (°)	123.1	123.1	122.8	123.5	123.7	123.7
γ (°)	90	90	90	90	90	90
a (Å)	116.8	116.5	116.6	117.4	118.1	118.1
b (Å)	38.2	37.6	38.7	38.5	38.7	38.7
c (Å)	97.1	95.4	95.4	97.0	96.5	96.5
Resolution (Å)	50-2.05 (2.15-2.04)	50-2.0 (2.08-1.99)	49-1.7 (1.79-1.71)	50-1.9 (1.96-1.86)	50-1.7	50-1.9(1.99-1.92)
# unique reflections	22,278	24,304	39,480	39980	37,876	24,234
Completeness (%)	92.7(70)	95.1(83)	98.2(88.9)	98.9(98.4)	96(85.2)	97.5(95.5)
I/σ	14.9(2.3)	22(2.9)	19.5(2.4)	16.4(3.3)	20.3(2.6)	13.0(3.6)
R_{merge}	0.068(0.450)	0.061(0.433)	0.077(0.52)	0.070(0.56)	0.057(0.48)	0.049(0.34)
Refinement						
R_{work}/R_{free}	19.1/23.0	17.0/20.1	17.5/20.3	18.8/21.9	19.7/21.4	23.3/27.2
B Factor	68.0	54.51	50.2	55.8	44.8	24.4
RMS bond length	0.014	0.011	0.011	0.008	0.010	0.006
RMS bond angle	1.528	1.435	1.487	1.179	1.328	1.065

GRγ-DBD:GBS 16bp and GR-DBD:GBS 18 bp Complexes

Data	**GRγ:FKBP5**	**FKBP5 – 18bp**		**Pal – 18bp**
Crystal Condition	34	52	67	36
Wavelength (nm)	1.11	1.283	1.00	1.00
	$C_1 2_1$	$P2_1 2_1 2_1$	$P2_1 2_1 2_1$	$P2_1 2_1 2_1$
α (°)	90	90	90	90
β (°)	122.8	90	90	90
γ (°)	90	90	90	90
a (Å)	115.7	39.7	39.1	39.1
b (Å)	39.7	101.3	100.2	102.1
c (Å)	95.2	112.5	112.5	112.1
Resolution (Å)	50-2.05 (2.14-2.05)	50-2.4 (2.48-2.38)	50-2.15 (2.22-2.15)	50-2.3 (2.40-2.32)
# unique reflections	24753	19913	31363	20142
Completeness (%)	95.3(73)	95.1(87.1)	98(99.9)	99.9(100)
I/σ	32.6(3.1)	19.3(2.3)	14.0(2.6)	23.1(3.9)

R_{merge}	0.05 (0.272)	0.100(0.508)	0.079(0.966)	0.079(0.615)
Refinement				
R_{work}/R_{free}	17.8/21.1	18.7/23.8	21.3/23.9	18.4/22.6
B Factor	73.66	57.4	64.8	58.1
RMS bond length	0.012	0.009	0.008	0.008
RMS bond angle	1.343	1.301	1.236	1.225

Supporting references.

S1. I. Rogatsky *et al.*, *Proc Natl Acad Sci U S A* **100**, 13845 (Nov 25, 2003).
S2. T. Meyer, J. A. Gustafsson, J. Carlstedt-Duke, *DNA Cell Biol* **16**, 919 (Aug, 1997).
S3. J. C. Wang *et al.*, *Proc Natl Acad Sci U S A* **101**, 15603 (Nov 2, 2004).
S4. J. A. Iniguez-Lluhi, D. Y. Lou, K. R. Yamamoto, *J Biol Chem* **272**, 4149 (Feb 14, 1997).
S5. I. Rogatsky, J. M. Trowbridge, M. J. Garabedian, *Mol Cell Biol* **17**, 3181 (Jun, 1997).
S6. L. Naldini *et al.*, *Science* **272**, 263 (Apr 12, 1996).
S7. S. Li *et al.*, *Cancer Res* **64**, 4833 (Jul 15, 2004).
S8. A. Y. So, C. Chaivorapol, E. C. Bolton, H. Li, K. R. Yamamoto, *PLoS Genet* **3**, e94 (Jun, 2007).
S9. E. C. Bolton *et al.*, *Genes Dev* **21**, 2005 (Aug 15, 2007).
S10. N. Collaborative Computational Project, *Acta Crystallogr D Biol Crystallogr.* **50**, 760 (1994).
S11. R. W. G.-K. P.D. Adams, L.-W. Hung, T.R. Ioerger, A.J. McCoy, N.W. Moriarty, R.J. Read, J.C. Sacchettini, N.K. Sauter and T.C. Terwilliger, *Acta Cryst.* **D58**, 1948 (2002).
S12. P. Emlsey, Cowtan, K., *Acta Crystallographica* **D60**, 2126 (2004).
S13. I. W. Davis *et al.*, *Nucleic Acids Res* **35**, W375 (Jul, 2007).
S14. E. F. Pettersen, Goddard, T.D., Huang, C.C., Couch, G.S., Greenblatt, D.M., Meng, E.C., and Ferrin, T.E., *Comput. Chem.* **25**, 1605 (2004).
S15. W. L. DeLano, *DeLano Scientific, Palo Alto, CA, USA.* (2002).
S16. S. C. Roemer *et al.*, *Mol Endocrinol* **20**, 3042 (Dec, 2006).
S17. T. N. Bhat, *J. Appl. Cryst.* **21**, 279 (1988).